Assessment of Construction Joint Effect in Full-Scale Concrete Beams by Acoustic Emission Activity

Dimitrios G. Aggelis[1]; Tomoki Shiotani[2]; and Masato Terazawa[3]

Abstract: In the present paper the mechanical and acoustic emission (AE) behaviors of full-scale reinforced concrete beams are evaluated. One of the beams was constructed in two parts, which were assembled later in order to evaluate the effect of the joints in the structural behavior. The load was applied by means of a four-point-bending configuration. It is revealed that at initial stages of loading, the conventional measurements of strain and deflection, as well as pulse velocity, do not show any discrepancy, although the structural performance of the two beams is eventually proven to be quite different. On the contrary, AE parameters, even from early load steps, indicate that the damage accumulation is much faster in the assembled beam. This is confirmed by the calculated sources of AE events which are close to the construction joints. The results show that the AE technique is suitable to monitor the deterioration process of full-scale structures and yields valuable information that cannot be obtained at the early stages of damage by any other way.

DOI: 10.1061/(ASCE)EM.1943-7889.0000130

CE Database subject headings: Acoustic methods; Concrete beams, cracking; Load bearing capacity; Reinforcement.

Author keywords: Acoustic methods; Concrete beams; Cracking; Fracture; Load bearing capacity; Reinforcement.

Introduction

The increase of the number of aging concrete structures worldwide is a certain fact. Their malfunction leads to large financial cost and, in some cases, it is catastrophic to human casualties as well. Therefore, damage assessment and maintenance are essential in order to secure or even extend the safe service life of structures. One of the techniques used for characterization of the integrity of structures is acoustic emission (AE).

Stressing a material above its strength results in cracking, giving rise to elastic waves propagating to all directions. These transient waves (AE signals) can be detected by AE sensors attached to the surface of the material. Analysis of the wave characteristics and origins can provide valuable information about the internal condition of the structure. The advantage of AE is the recording of the damage process during the entire load history, which enables to determine the onset of fracture and follow all the subsequent stages. In laboratory studies, AE parameters have been correlated with the damage process and failure modes (Schechinger and Vogel 2007; Ohtsu et al. 2002; Shiotani et al. 1999, 2001, 2003; Mihashi et al. 1991; Grosse et al. 1997; Grosse and Finck 2006; Triantafillou and Papanikolaou 2006). There are also applications of AE in actual structures with the aim of damage quantification or repair evaluation (Ohtsu et al. 2002; Shiotani et al. 2001, 2004a,b, 2005, 2006).

In the present paper, the mechanical and AE behavior of two full-scale 6.5 m reinforced concrete beams under bending is discussed. The aim was the comparison between two different construction methods: one beam was constructed as one piece, while the second had been two separate pieces were joined later. The beams were loaded in four-point bending and besides mechanical parameters, such as load, deflection and strain, AE was recorded as well. The obvious advantage of the "connected" beam is easier handling in situ. The actual application in mind was ground support for tunnel construction underneath railways. However, before this type of construction could be safely adopted in practice, its performance should be evaluated. The importance of this work is that the elements which are mechanically tested and monitored by AE have the same size as the ones used in situ and therefore, the actual behavior was examined without assumptions about the size effect. It is mentioned that laboratory tests of full-scale concrete elements of this size, accompanied by AE monitoring are rare in literature.

AE

In this section a brief description of AE parameters that will be studied throughout the paper will take place. After a specific crack propagation incident, all the waveforms recorded (*hits*) are parts of an *AE event*. The time delay of arrival to the different transducers is used to calculate the position of the event source, provided that the pulse velocity of the material is known. Practically, this means that after any AE event, the position of the source crack can be calculated.

Some very important parameters of AE are the number of AE hits or events and their intensity, measured by the peak amplitude of the waveforms. At the early stages of damage the number of emissions is limited and their intensity is low. As the stress in-

[1]Assistant Professor (Contract), Dept. of Materials Science and Engineering, Univ. of Ioannina, Ioannina 45110, Greece (corresponding author). E-mail: daggelis@cc.uoi.gr

[2]Associate Professor, Dept. of Urban Management, Graduate School of Engineering, Kyoto Univ., C1-2-236, Kyoto-Katsura, Nishikyo-ku, Kyoto 615-8540, Japan. E-mail: shiotani@toshi.kuciv.kyoto-u.ac.jp

[3]■, Civil Engineering Headquarters, Tobishima Corp., 2-Banchi, Sanbancho, Chiyoda-ku, Tokyo 102-8332, Japan. E-mail: masato_terazawa@tobishima.co.jp

Note. This manuscript was submitted on December 3, 2009; approved on December 17, 2009; published online on XXXX XX, XXXX. Discussion period open until December 1, 2010; separate discussions must be submitted for individual papers. This paper is part of the ***Journal of Engineering Mechanics***, Vol. 136, No. 7, July 1, 2010. ©ASCE, ISSN 0733-9399/2010/7-1–XXXX/$25.00.

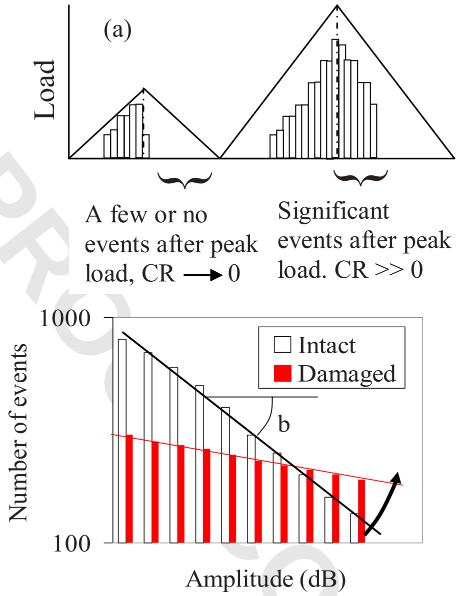

Fig. 1. (a) Representation of AE activity with damage process. The bars stand for AE event rate. (b) Peak amplitude distribution. The I*b* value is the absolute slope.

creases and the damage propagates, the number of emissions generally becomes larger, as well as their amplitude (Shiotani et al. 1999, 2001, 2004a, 2005; Schechinger and Vogel 2007; Ohtsu et al. 2002).

For damage quantification purposes, certain indices have been proposed. As stated earlier, when a material or structure is stressed, AE is produced. Additionally, the behavior during unloading is also crucial. In the case where the material is intact (or the applied load is low), the AE activity during unloading is of low intensity, as seen in Fig. 1(a). For damaged material though, the emissions are intense even during unloading, see again Fig. 1(a). The number of AE events during unloading divided by the number of events during the whole cycle is defined as the *calm ratio* and values near 0 indicating intact material condition (Ohtsu et al. 2002; Shiotani et al. 2004a,b, 2006; Colombo et al. 2005).

Another index comes from the analysis of the amplitude distribution of the events, or the so called improved *b* value (I*b* value for short) (Shiotani et al. 1994). While in general, a large scale of the fracture corresponds to large AE peak amplitude, the use of the amplitude solely can be misleading. This is because the accumulated damage increases the material attenuation due to scattering on the cracks. Therefore, even strong signals will be severely attenuated before being recorded by the sensors. To avoid confusion, the amplitudes are studied through their cumulative distribution that changes as the damage is accumulated [see Fig. 1(b)]. Specifically, the gradient of the distribution is calculated. With the evolution of damage this slope decreases, meaning simply that from the total population of events, the percentage of the strong ones increases relatively to the weak. It has been confirmed that at the moments of extensive cracking, the I*b*-value exhibits severe drops (Shiotani et al. 1994, 2001, 2004a,b; Kurz et al. 2006; Colombo et al. 2003).

The location of the AE events revealed the sensitive areas of each design that acted as crack initiators. Also, the aforementioned AE indices indicated which beam was more critically damaged even from the first cycle of the loading process. Strain and deflection are also briefly discussed exhibiting discrepancies between the two beams only at the final stage of failure.

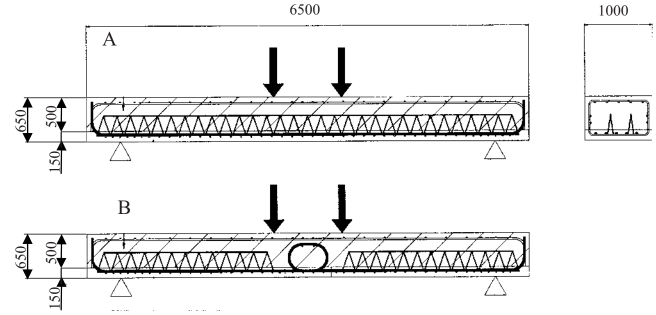

Fig. 2. Geometry and reinforcement arrangement of the beams

Concrete Beams

The geometry of the beams with a rough sketch of the reinforcement can be seen in Fig. 2. The length was 6.5 m while the cross section was 0.65 m (height) by 1 m. They consist of two layers of concrete. The lower had a thickness of 150 mm, containing aggregates of maximum size of 20 mm. The water to cement ratio by mass was 0.53 and the amounts of cement, water, sand, and aggregates in a cubic meter were 299, 159, 800 and 1,080 kg, respectively. After the complete hydration of this layer (at 28 days) the second layer was cast on top. This layer had larger aggregates of 100 mm and quick setting, and hardening grout was used with water to cement ratio by mass $W/C=0.22$.

The basic difference of the two beams was the construction process. The first (Beam A) was constructed in a unified way, i.e., each layer was cast as one piece. On the other hand, the bottom layer of Beam B was constructed in two separate parts that were joined together during the casting of the upper layer, see representation of Fig. 3.

Mechanical Testing

The beams were loaded in a four-point-bending test. The overall span between the supports was 6 m, and the load was applied from the top surface as seen in Fig. 4. Several strain gauges and deflection meters were attached to the surface of concrete, as well as on the reinforcement bars before casting. The loading consisted of five cycles: the first two were up to 500 kN, the third and fourth were up to 750 kN, and the last was up to failure.

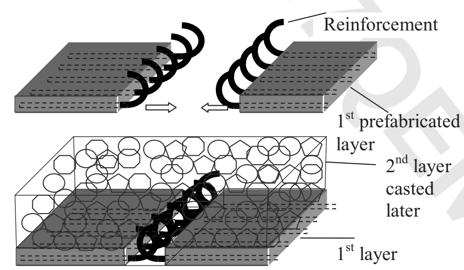

Fig. 3. Detail of the assembly of Beam B

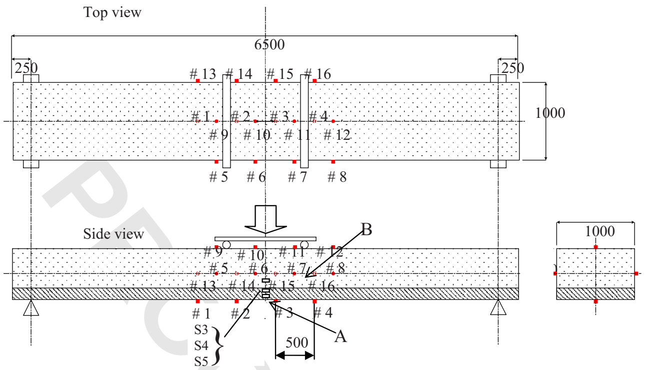

Fig. 4. Geometry of the experiment and sensor location

AE Monitoring

Sixteen piezoelectric sensors R6 of physical acoustics (PAC) were employed for the AE monitoring. The specific sensors exhibit high sensitivity at the band below 100 kHz and are widely used in AE monitoring projects. They were attached using electron wax on Positions 1–16, as shown in Fig. 4. The signal was preamplified by 40 dB, digitized with a sampling rate of 1 MHz and stored in a PAC, DiSP 16 channel system. Apart from the analysis of parameters and waveforms, the software AEWin of PAC provided automatic, real-time event source location during the experiment.

Mechanical Behavior

The purpose of the present paper is to focus more on the AE parameters and therefore, from the total number of 55 strain gauges and five deflection meters only some indicative results will be presented. In Fig. 5, the load versus deflection curves can be observed for both beams. This deflection was measured at the lower center point of each beam, see Point A in Fig. 4. The behaviors of both beams are similar in general. The slopes of the curves do not show significant discrepancies. The most important observation concerns the maximum load. It is clear that Beam A withstood higher load, specifically 1,014.5 kN, while Beam B reached to a maximum of 917.5 kN. The maximum deflection of Beam A was also higher (72 mm compared to 65.6 mm of Beam B), implying that the structure of Beam A absorbed higher energy before failure.

In Fig. 6 one can observe the load versus strain behavior, as measured by strain gauges placed on the top side of concrete, see Point B in Fig. 4. Since the top surface undergoes compression, the strain values are negative. The maximum strain is again higher for Beam A ($2{,}081\mu$ compared to $1{,}630\mu$ of Beam B). In any case, from Figs. 5 and 6, a large permanent plastic deformation is obvious, resulting in a deflection of the midspan of 40 to 50 mm even after the final unloading.

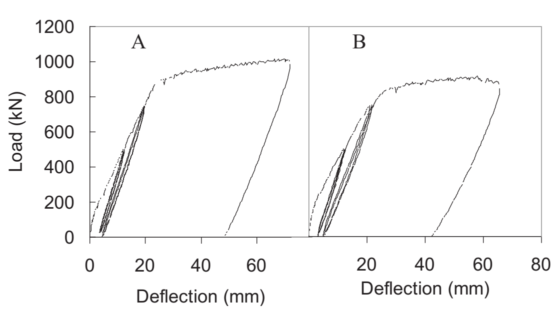

Fig. 5. Load versus center deflection curves for both beams

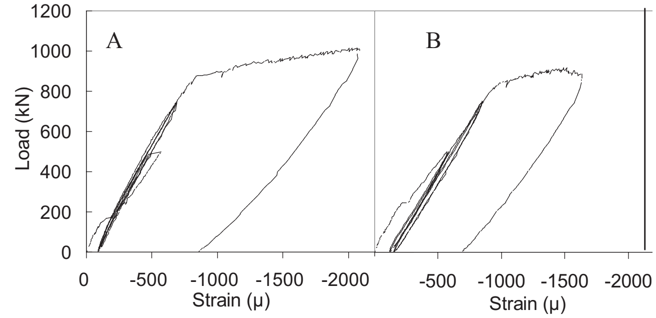

Fig. 6. Load versus top center strain curves for both beams

The evaluation of the behavior comes after comparison of the final values for the two beams and could not be used as an absolute measure of deterioration at early ages. To this end, AE activity helps in the quantification and localization of damage even at low stress levels.

AE Results

In Fig. 7 one can see the time history of the cumulative number of AE events along with the applied load for Beams A and B, respectively. As seen, the AE events are recorded shortly after application of the load. During any cycle of loading and unloading the events increase, finally reaching for Beam B a number more than double to that compared with Beam A. This is by itself an indication of more intense cracking that happened in the joint Beam B. What is more important though, is the value of AE indices, like the calm ratio that was mentioned earlier. In Table 1, the numbers of events during the loading and unloading process of Steps 1 and 3 are presented. The activity of B was intense even

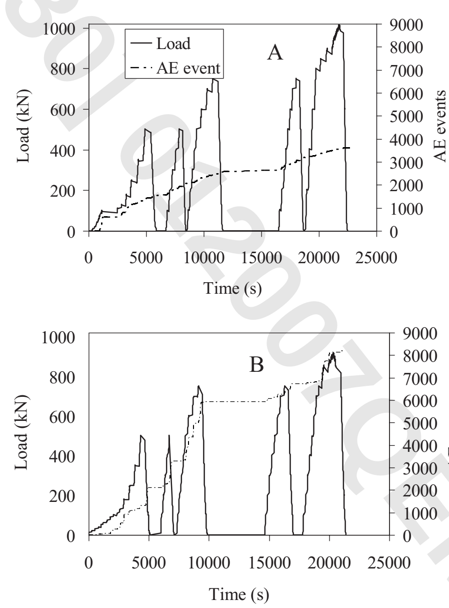

Fig. 7. Time history of load and cumulative AE events for Beams A and B

AQ: #4

Table 1. Number of Events during Loading-Unloading Steps and Calm Ratio

	Beam A			Beam B		
	Loading	Unloading	Calm ratio	Loading	Unloading	Calm ratio
First step (500 kN)	1412	121	**0.079**	1286	807	**0.386**
Third step (750 kN)	390	117	**0.230**	1718	934	**0.352**

Note: Boldface font=

from the first unloading (maximum load of 500 kN). The number of the events during unloading was almost of the same order with loading, leading to a calm ratio of 0.39. This value is related with high degree of damage in relevant works (Ohtsu et al. 2002; Shiotani et al. 2004a,b, 2005, 2006; Colombo et al. 2005) and shows that the damage of Beam B was extensive even from the first loading cycle. In the aforementioned literature an empirical threshold value of 0.05 is defined, above which severe deterioration is implied. Under these circumstances, small fluctuations of calm ratio above 0.3 are considered insignificant. On the contrary, Beam A exhibited much less activity during unloading and therefore lower calm ratio. At the third step however, Beam A also exhibited high calm ratio (0.23), implying that at this point it was seriously damaged as well.

Event Location

It is interesting to focus on the location of the events. In Fig. 8 one can observe the location of the events for the first loading and unloading step for beam A along with the pattern of surface cracks developed. The events are indicated by circles, the center of which is the location of the source, and the diameter stands for the amplitude of the first detected signal of the event. A pattern can be distinguished, implying a zone from approximately 0.15 m on the left extending diagonally to the top. However, in general the events seem well distributed to the whole volume, not showing a particularly strong preference. During unloading, the number of events is certainly lower indicating small damage.

Concerning Beam B, see Fig. 9, most of the events are located above the position of the left joint. This means that the joint contributed to local stress concentration leading to accumulation of cracks. Near the left joint, at both sides, visible surface-breaking cracks were developed, one of which propagated more than 400 mm to the top, being very close to the calculated event sources, as can be seen in Fig. 9. Even more indicative is the behavior during unloading, as seen in the lower part of Fig. 9. It is clear that a large number of events were nucleated again from the area above the construction joint, most of them having high intensity. The above shows that the construction joint contributed to local stress concentration, leading to extensive cracking at the area close and above the construction joint. This led to the much lower strength exhibited eventually. It is interesting to observe that the area away from the left joint exhibited smaller activity. Even if the structure and the load is symmetric, after the first crack is developed at a strong candidate point (i.e., the left joint in this case), the stress is released and therefore, it is reasonable that the rest of the area, including the right joint, would not exhibit similar activity, as also seen in Fig. 9. In any case, although the number of events at the right joint is less, their intensity is high, as will be seen in the next paragraph.

In Fig. 10 the total energy of the AE events for different load stages is presented according to the horizontal position of the event epicenter. For this figure, the monitored area was divided to vertical zones of 100 mm each, and the energy of all individual events that occurred within each zone was summed. The energy of the individual signals was measured by the area under the rectified signal envelope that is closely related to the energy of the source (Shiotani et al. 2001).

AE energy is widely distributed for Beam A. Gradually, with each cycle, accumulation of energy is observed at the zone around 0.15 m from the left. At that point, visible cracks developed even from the first cycle, as seen Fig. 8.

For Beam B, the energy was located at the zones of 0.55 m, as

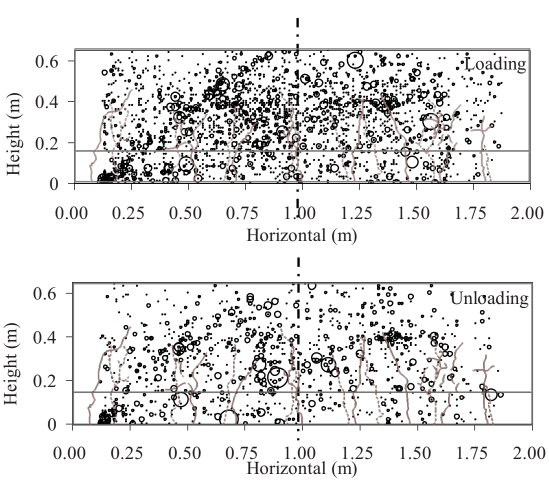

Fig. 8. Location of AE events and surface crack pattern for the first loading cycle for Beam A. The solid lines denote cracks observed on the front side and dashed lines on the rear side and the dashed-dotted centerline of the specimen.

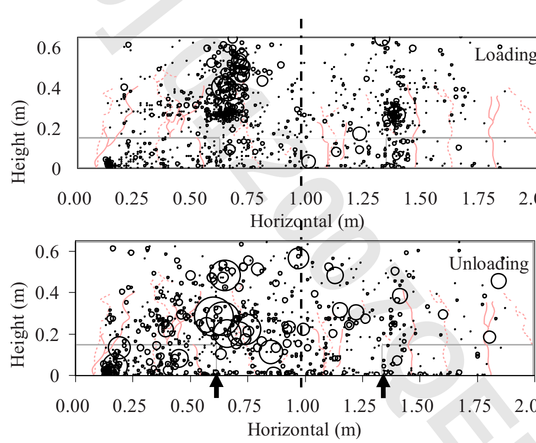

Fig. 9. Location of AE events and surface crack pattern for the first loading cycle for Beam B. The arrows indicate the connection between the two layers. The solid lines denote cracks observed on the front side and dashed lines on the rear side and the dashed-dotted centerline of the specimen.

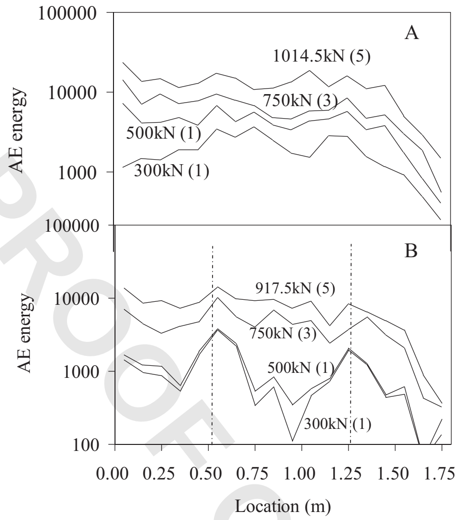

Fig. 10. AE energy versus horizontal location for Beams A and B. The number in parentheses indicates the loading cycle. The vertical dashed-dotted lines correspond to the position of the joints of Beam B.

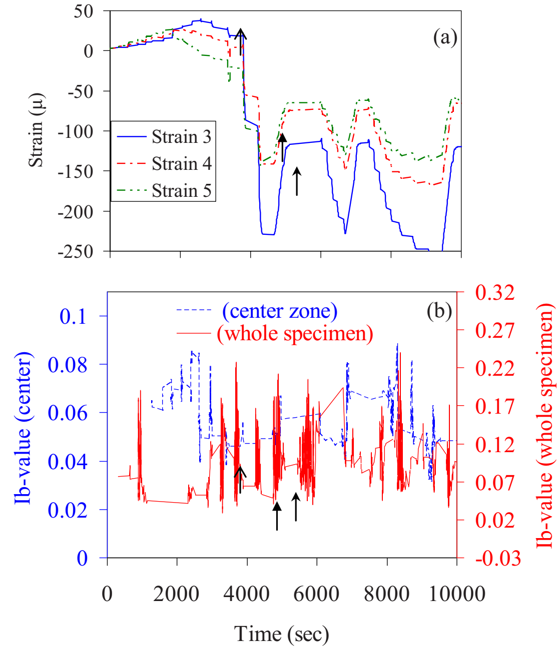

Fig. 11. Time history of (a) strain; (b) I*b*-values for beam B

well as 1.35 m from the start. These zones correspond to the positions of the joints between the two different materials, showing again that the joints acted as crack initiators. As seen earlier in Fig. 9, the left joint had more intense activity; however there is also a local maximum of AE energy at the vicinity of the right joint, revealing that it also contributed to fracture from the first cycle. After this initial cycle that led to extensive cracking at these locations, AE energy started to emerge from the zone of 0.15 m, near which a surface-breaking crack was observed, similar to Beam A (see Figs. 8 and 9).

In inhomogeneous structures like the ones described herein, the pulse velocity is not constant for any propagation direction. This reduces the accuracy of event location. Therefore, it is reasonable that the center of the events is not located exactly on the visible pattern of the cracks. Additionally, if some major cracks develop, this could hinder the recording of signals from other cracks since the straight propagation path to some sensors is disrupted. This is a reason why many visible surface-breaking cracks are not accompanied by AE events in the near vicinity. It is not within the scope of the manuscript to discuss the algorithms used for localization. In any case however, the accuracy of localization cannot be constant and depends on a number of parameters: the onset picking algorithm, the AE source localization algorithm (Grosse et al. 1997), the propagation velocity, and the location of the sensors (Schechinger and Vogel 2007). The effect of velocity will be briefly discussed later.

I*b*-Value and Strain

As mentioned earlier, extensive cracking influences temporarily the AE event amplitude distribution. In case strain gauges are in the near vicinity of the crack, a sudden change can be seen in the strain behavior as well. Such a case is presented in Fig. 11(a) for Beam B. There, the time histories of three individual strain gauges (S3, S4, and S5 of Fig. 4) are depicted for the first three hours of the experiment. All of them are positioned clearly below the neutral axis, so normally they should exhibit positive (tensile) strain. After about 2,500 s the strain readings start to change direction and in the time span of 3,800 to 4,250 s they exhibit a severe decrease, becoming negative while the load was still monotonically increasing. These moments are pointed by the arrows. These changes of the strain are attributed to extensive cracking that occurred near the strain gauges and were recorded by all of the three strain gauges in the vicinity.

Focusing on the time history of the I*b*-value from events located in the whole volume, it is seen that it exhibits many points of fluctuation throughout the experiment, indicating different cracking events, see solid line of Fig. 11(b). Any sudden change is the result of crack propagation events, as explained earlier. At the time of 3,800 and 4250 s these fluctuations (marked again by similar arrows) accompany the severe changes of measured strain, as presented in Fig. 11(a). Additionally, concentrating only on the events located within a center zone of 300 mm (dashed line), where also the strain gauges were attached, a sudden change of I*b* value is exhibited at the time of 2,500 s where the readings of the strain gauges start to change direction. The I*b* value at that point exhibited a significant drop from 0.085 to 0.04. Therefore, the reason which led to rapid changes in strain readings (cracking incidents), also resulted in fluctuations of the I*b* value. Furthermore, the I*b* value of the center zone dropped below 0.05 in many cases in Fig. 11(b). This value has been related to extensive damage by previous studies (Shiotani et al. 1994, 2001, 2004) and is another indication of the severe condition of the joined beam, even from the first loading cycle. It is mentioned that as the load increases, the whole beam is continuously deteriorating. However, the I*b* value cannot monotonically decrease; after any crack propagation incidence, the crack tip reaches material volumes which were healthy some milliseconds before. Therefore, until the crack propagates again, the I*b* value may well increase and definitely exhibit some fluctuations, as seen in Fig. 11(b).

The above demonstrates the capability of AE to monitor the fracture process in a large area using a number of sensors at positions even away from the location of damage. On the contrary, the conventional gauges can indicate the cracking process only if they are located close to the crack (such as S3, S4, and S5

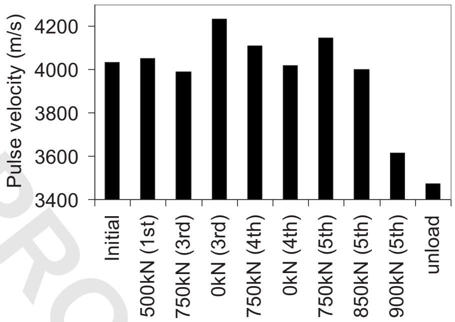

Fig. 12. Average pulse velocity for different load stages

in this case). However, in an actual structure this cannot always happen since the accurate position of the cracks cannot be known a priori.

Pulse Velocity Measurements

As mentioned in the introduction, in order to accurately calculate the location of the events, the pulse velocity must be known. The structures of this study are highly inhomogeneous, with two layers of concrete, different aggregates for each layer and densely reinforced by steel bars. When an AE event takes place, the energy propagates possibly through different concrete layers and a number of reinforcing bars before reaching the sensors' position. Therefore, strictly speaking, there is not a single pulse velocity characteristic of the beams. Depending on the direction, each hit may propagate with different velocity. This certainly induces an error in the location of AE sources. In the present case, in order to minimize this error, many wave paths were measured and the values were averaged before the start of the experiment. An additional error is induced during the different loading stages, as the velocity changes due to cracking of the microstructure. In order to examine if the changes of velocity influence the location of AE events significantly, velocity measurements were conducted during the different loading stages for the Beam B. This was done using a ball impact from a constant height near the position of Sensor 5, see Fig. 4, that acted as trigger. The transit time to all other sensors was measured and the velocity was calculated as the average of the individual velocities. In Fig. 12 one can see the average velocity at some major steps of the experiment. The velocity had fluctuations up to 5% of the initial value, even positive, something that has been mentioned in other relevant cases (Suaris and Fernando 1987; Popovics and Popovics 1991). This has been attributed to the pressure that consolidates the medium and facilitates the wave propagation. Only at the final stage, the velocity exhibited a constantly decreasing trend. Specifically, at 900 kN of the last loading, the velocity reduced by 10% and after the eventual failure at 917.5 kN, it was further reduced by 14%.

After an AE event occurs in the structure, considering the cross section of the beams and the position of the sensors, the wave will propagate less than 0.4 m before being recorded by a sensor. Therefore, the velocity fluctuation of 5% (throughout most of the experiment) may alter the transit time to the sensor and therefore, the location calculation by the same percentage (or approximately 20 mm). However, taking into account that the same event will be recorded by a number of other sensors, it is not easy to calculate exactly how much this error will be reduced. The problem becomes more complicated, considering other sources of error, as, for example, that of the onset picking algorithm (Schechinger and Vogel 2007; Kurz et al. 2005).

Although the velocity itself is not assumed to impose large localization error, it was confirmed that it is not sensitive to the damage, since even at the last cycle and at the load of 850 kN, the velocity was of the same level with that of in the initial (above 4,000 m/s).

Conclusions

In the present paper the mechanical performance and AE activity of two full-scale concrete beams is studied. One of them had been constructed as two parts which were joined later. The purpose was to evaluate the load bearing capacity relatively to the construction joint. AE results showed that the joints acted as crack initiators, and significant damage was accumulated in their vicinity from the early stages of loading. This was indicated by the location of AE events, while the activity during unloading, quantified by the calm ratio, confirmed the extend of damage. As a result, the assembled beam withstood 10% lower load compared to the monolithic one in the bending test. This lower load-bearing capacity, as well as concerns about the long-term behavior (given the early cracking during the experiment) halted the production of this type of structure. The AE amplitude distribution quantified by the I*b* value indicated the crack propagation events, something that strain and deflection gauges cannot monitor unless the fracture occurs in their vicinity. Moreover, the mechanical measurements did not exhibit noticeable discrepancies between the two beams during the early loading stages, while the only difference was obtained close to failure. AE analysis shows the ability to monitor large volume, with real-time crack localization, as well as correlation of cracking process with the applied load even from the early stages of damage.

References

Colombo, S., Forde, M. C., Main, I. G., and Shigeishi, M. (2005). "Predicting the ultimate bending capacity of concrete beams from the 'relaxation ratio' analysis of AE signals." *Constr. Build. Mater.*, 19, 746–754.

Colombo, S., Main, I. G., and Forde, M. C. (2003). "Assessing damage of reinforced concrete beam using 'b-value' analysis of acoustic emission signals." *J. Mater. Civ. Eng.*, 15(3), 280–286.

Grosse, C., Reinhardt, H., and Dahm, T. (1997). "Localization and classification of fracture types in concrete with quantitative acoustic emission measurement techniques." *NDT Int.*, 30(4), 223–230.

Grosse, C. U., and Finck, F. (2006). "Quantitative evaluation of fracture processes in concrete using signal-based acoustic emission techniques." *Cem. Concr. Compos.*, 28(4), 330–336.

Kurz, J. H., Finck, F., Grosse, C. U., and Reinhardt, H. W. (2006). "Stress drop and stress redistribution in concrete quantified over time by the b-value analysis." *Struct. Health Monit.*, 5, 69–81.

Kurz, J. H., Grosse, C. U., and Reinhardt, H. W. (2005). "Strategies for reliable onset time picking of acoustic emission and of ultrasound signals in concrete." *Ultrasonics*, 43(7), 538–546.

Mihashi, H., Nomura, N., and Niiseki, S. (1991). "Influence of aggregate size on fracture process zone of concrete detected with three dimensional acoustic emission technique." *Cem. Concr. Res.*, 21, 737–744.

Ohtsu, M., Uchida, M., Okamoto, T., and Yuyama, S. (2002). "Damage assessment of reinforced concrete beams qualified by acoustic emission." *ACI Struct. J.*, 99(4), 411–417.

Popovics, S., and Popovics, J. S. (1991). "Effect of stresses on the ultrasonic pulse velocity in concrete." *Mater. Struct.*, 24, 15–23.

Schechinger, B., and Vogel, T. (2007). “Acoustic emission for monitoring a reinforced concrete beam subject to four-point-bending.” *Constr. Build. Mater.*, 21(3), 483–490.

Shiotani, T., Bisschop, J., and Van Mier, J. G. M. (2003). “Temporal and spatial development of drying shrinkage cracking in cement-based materials.” *Eng. Fract. Mech.*, 70(12), 1509–1525.

Shiotani, T., Fujii, K., Aoki, T., and Amou, K., (1994). “Evaluation of progressive failure using AE sources and improved b-value on slope model tests.” *J. Acoust. Emiss.*, VII(7), 529–534.

Shiotani, T., Luo, X., and Haya, H. (2006). “Damage diagnosis of railway concrete structures by means of one-dimensional AE sources.” *J. Acoust. Emiss.*, 24, 205–214.

Shiotani, T., Nakanishi, Y., Iwaki, K., Luo, X., and Haya, H. (2005). “Evaluation of reinforcement in damaged railway concrete piles by means of acoustic emission.” *J. Acoust. Emiss.*, 23, 260–271.

Shiotani, T., Nakanishi, Y., Luo, X., and Haya, H. (2004b). “Damage assessment in deteriorated railway sub-structures using AE technique.” *J. Acoust. Emiss.*, 22, 39–48.

Shiotani, T., Nakanishi, Y., Luo, X., Haya, H., and Inaba, T. (2004a). “Damage evaluation for railway structures by means of acoustic emission.” *Key Eng. Mater.*, 270–273, 1622–1630.

Shiotani, T., Ohtsu, M., and Ikeda, K. (2001). “Detection and evaluation of AE waves due to rock deformation.” *Constr. Build. Mater.*, 15(5–6), 235–246.

Shiotani, T., Shigeishi, M., and Ohtsu, M. (1999). “Acoustic emission characteristics of concrete piles.” *Constr. Build. Mater.*, 13, 73–85.

Suaris, W., and Fernando, V. (1987). “Detection of crack growth in concrete from ultrasonic intensity measurements.” *Mater. Struct.*, 20, 214–220.

Triantafillou, T. C., and Papanikolaou, C. G. (2006). “Shear strengthening of reinforced concrete members with textile reinforced mortar (TRM) jackets.” *Mater. Struct.*, 39(1), 93–103.

AUTHOR QUERIES — 012007QEM

#1 Au: Please check that ASCE Membership affiliations are provided for all authors that are members.
#2 Au: Please supply the author role for the third author in the affiliations.
#3 Au: Please check all grammar edits to ensure that your meaning was preserved.
#4 Au: Please verify the boldfaced characters in table 1 and please define what said characters mean in table note.